

# Self-correction phase transition in the dissipative toric code

Sanjeev Kumar\* and Hendrik Weimer

*Institut für Physik und Astronomie, Technische Universität Berlin,  
Hardenbergstraße 36, EW 7-1, 10623 Berlin, Germany*

(Dated: February 24, 2026)

We analyze a time-continuous version of a cellular automaton decoder for the toric code in the form of a Lindblad master equation. In this setting, a self-correcting quantum memory becomes a thermodynamical phase of the steady state, which manifests itself through the steady state being topologically ordered. We compute the steady state phase diagram, finding a competition between the error correction rate and the update rate for the classical field of the cellular automaton. Strikingly, we find that self-correction of errors is possible even in situations where conventional quantum error correction does not have a finite threshold.

## I. INTRODUCTION

The long-term preservation of quantum information is one of the key requirements to build a scalable quantum computer [1–3]. This had led to the development of sophisticated error correction algorithms to combat unavoidable imperfections during the operation of the device [4–12]. Here, we connect these efforts to the emerging field of open quantum many-body systems [13–42] and show that a dissipative variant of the toric code exhibits a self-correcting phase that can be used for long-term information storage.

Quantum error correction algorithms are routinely characterized in terms of their error correction threshold, which refers to the maximum strength of a depolarizing noise channel applied to one of the logical states that still can be corrected [43]. While this assumes a static and uncorrelated application of the noise, real-world quantum devices are complex dynamical systems potentially exhibiting emergent errors that cannot be understood purely from a microscopic set of rules [44–46]. Such a viewpoint is much closer to the notions of open quantum many-body systems, where the long-term behavior of quantum systems is characterized in terms of thermodynamic phases of the steady state and phase transitions between them [21, 47–49].

In this article, we provide a synthesis between the fields of quantum error correction and open quantum many-body systems. Specifically, we consider a dissipative variant of the toric code model that is governed by microscopic Lindblad dynamics [50, 51]. The Lindblad jump operators are structured in such a way that they implement a cellular automaton decoder for the toric code [52–55] and hence have the ground states of the toric code as their dark states. In order to be able to fuse distant anyon excitations by purely local jump operators, the rates for the quantum jumps are controlled by the value of a classical field that is updated according to the local anyon densities, in a similar way as it has already been discussed for conventional error correction algorithms [56, 57]. To

introduce errors, we consider the appearance of local bit and phase flip errors; however, the subsequent evolution naturally generates more complex error syndromes. We then analyze the steady state of the dynamics and show that the dynamics is capable of self-correction provided the state remains in the topologically ordered phase according to a recently introduced operational definition of topological order [58]. We map out the steady state phase diagram by varying the relative strengths of the error rates and field-update rates, respectively. Crucially, we find a stable quantum memory even when the classical field is two-dimensional, in contrast to the conventional error correction scenario [59–62].

## II. DISSIPATIVE TORIC CODE

### A. The toric code model

The toric code [63, 64] is a paradigmatic model for a topological quantum memory. In its Hamiltonian formulation, it can be expressed as a sum of vertex and plaquette operators

$$H = - \sum_{v \in \text{vertices}} A_v - \sum_{p \in \text{plaquettes}} B_p \quad (1)$$

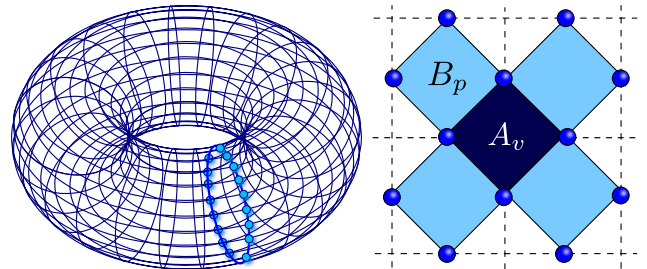


FIG. 1. Schematic of the toric code. Left: Spins are placed on the surface of a torus, with the highlighted nontrivial loop corresponding to an operation changing the logical value of the stored information. Right: The surface is structured according to a checkerboard pattern of vertex operators  $A_v$  and plaquette operators  $B_p$  involving the adjacent four spins of each vertex and plaquette, respectively.

\* sanjeev.kumar@tu-berlin.de

wherein the two operators are defined in terms of Pauli's acting on spin-1/2 particles on the edges of a two-dimensional (2D)  $L \times L$  periodic lattice as shown in Fig. 1. The vertex and plaquette terms are given by

$$A_v = \prod_{i \in v} \sigma_i^x \quad B_p = \prod_{i \in p} \sigma_i^z, \quad (2)$$

respectively. Owing to the mutual commutativity of the operators with  $H$ , the ground state(s) correspond to the state space with  $A_v = B_p = 1 \forall v$  and  $p$ .

### B. Errors in the toric code

Local perturbations can violate the constraints on  $A_v$  and  $B_p$ , causing excitations above the ground state. For instance, a qubit-flip at site- $i$  on account of local  $x$ -perturbation,  $\sigma_i^x$  would update the two adjacent neighbouring plaquettes to  $B_p = -1$ . These excitations at the two plaquettes lead to nontrivial quasiparticles, known as anyons. The two anyons can be thought of as being attached to each other by a string via the perturbed qubit- $i$ . At no further energy cost, the anyons along with their string can diffuse further around the lattice, eventually resulting in either a topologically trivial loop and vanishing or in the worst case forming a topologically non-trivial loop around the lattice. In the latter case, logical error is said to have occurred, with the quantum system being in a different ground state orthogonal to the initial ground state. Location of anyons are detected from stabilizer measurements ( $B_p$  in this case). Quantum error correction therefore intends to pair-up these anyons forming trivial string loops, and eliminate them altogether.

A similar description follows for another kind of anyons emerging from  $z$ -perturbation or equivalently,  $A_v = -1$ . The two kinds follow braiding statistics with one another. We focus on the uncorrelated  $x$ - and  $z$ -perturbations scenario, where studying one kind suffice due to the dual nature of the problem.

### C. Cellular Automaton decoder

In the following, we consider a dynamical system where errors are continuously created and removed by different processes. The error correction dynamics is performed by constructing a coupled *quantum-classical* system, where an open quantum system is coupled to a cellular automaton (CA). Based on local update rules, the classical CA guides the dynamics of the anyons in the quantum toric code. We establish the Lindbladian dynamics of the coupled system which involve the following processes: anyon-pair creation, anyonic motion based on the CA field, and CA field-update. The anyon motion and CA field-update are closely related to the operations arising in the conventional error-correction using a CA field [52, 53]. Below, we describe the three processes:

#### 1. Anyon-pair creation

$$E_j = \sigma_j^x \quad (3)$$

The Pauli operator  $\sigma^x$  at the  $j^{\text{th}}$ -spin creates anyons on the adjacent plaquettes. We note that adding vertex violations in the form of  $\sigma^z$  errors only changes the steady state properties quantitatively, as the vertex violations would be updated independently. The qualitative behavior of the steady state phase diagram will remain unchanged. To prevent the computational cost of our simulations becoming prohibitively large, we focus on  $\sigma^x$  errors or plaquette violations only. We note that repeated action of  $E_j$  on neighboring plaquettes will also introduce diffusive motion of the anyons.

#### 2. Anyon motion

$$T_{pp'} = \sigma_j^x \left( \frac{1 - B_p}{2} \right) w_{p'} \quad (4)$$

The anyon, if present at plaquette  $p$ , transfers to a neighbouring plaquette  $p'$  with a probability determined by the weight factor  $w_{p'}$ . Crucially,  $w_{p'}$  depends on the values of the CA field  $\phi_{p'}$  at the neighboring plaquette. We choose  $w_{p'} = 1$  for the neighbor  $p'$  having the largest field value  $\phi_{p'}$  and  $w_{p'} = 0$  for all other neighbors. This means that the anyons are moving towards the largest value of the CA field.

#### 3. CA field-update

$$\phi'_p = \phi_p^{\text{avg}} + \frac{1 - \mathcal{B}_p}{2} - \Delta \quad (5)$$

Here,  $\phi'_p$  denotes the updated field value at  $p$ ,  $\phi_p^{\text{avg}}$  is the average of the field value of the nearest-neighbours of  $p$ , and  $\mathcal{B}_p$  is the measurement result obtained by measuring the operator  $B_p$ . The penalty term  $\Delta = \phi_p/L^2$  is introduced to regularize the growth of the field, preventing a monotonous increase in the long-time limit. Modulo  $\Delta$ , the field value at  $p$  updates to average of the field values of neighbours when anyon is absent at  $p$ , otherwise it updates to average plus one. While being local, the field-update term spreads the local information outwards and the additional one term attracts the anyons in the vicinity via the anyon motion process of Eq. (4). The CA field is initialized in the state  $\phi_p \equiv 0$ .

These processes can also be realized in a time-continuous form using a quantum master equation in Lindblad form. Specifically, the dynamics is governed by

$$\frac{\partial \rho}{\partial t} = \sum_i \left( L_i \rho L_i^\dagger - \frac{1}{2} \{ L_i^\dagger L_i, \rho \} \right) \quad (6)$$

where the sum runs over all the Lindbladian processes. The Lindblad operators  $L_i$  are chosen from the set

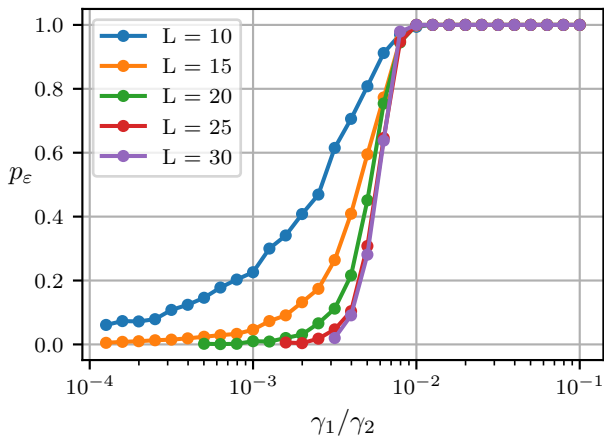


FIG. 2. Logical error probability  $p_\varepsilon$  in the steady state depending on the error rate  $\gamma_1$  for different system sizes  $L \times L$ . The field-update rate is taken as  $\gamma_3 = 10\gamma_2$ . Each data point is an average obtained from  $10^3$ -simulation runs. The simulation points to a critical error rate of about  $\gamma_1 = 10^{-2}\gamma_2$ , below which logical errors are increasingly suppressed with system size.

$\{E_j, T_{pp'}\}$ , while at the same time the CA field is updated according to Eq. (5). In the following, we use  $\gamma_1$ ,  $\gamma_2$ , and  $\gamma_3$  for anyon-pair creation, anyon motion, and CA field-update rates, respectively.

Crucially, the master equation in the absence of error production, i.e.,  $\gamma_1 = 0$ , has the four ground states of the toric code as dark states leading to  $\partial_t \rho = 0$ . Switching on  $\gamma_1$  will perturb these states, with the central question being whether the errors are capable to introduce nontrivial loops around the torus corresponding to logical errors of the toric code. In particular, the question whether the dynamics is capable to correct its own errors establishes its own thermodynamic phase, which we will refer to as the *self-correction phase* in the following. Establishing error correction as a thermodynamic phase allows to use the rich machinery of quantum many-body physics to analyze its properties and its disappearance in the form of a phase transition.

Finally, we note that the master equation can be unravelled in the anyon basis onto a set of pure states  $[\{B_p\}, \{A_v = 1\}, \lambda]$ , with  $\lambda$  being a topological quantum number [65]. Since these states do not contain any superposition in this basis, the dynamics can be simulated efficiently, allowing to reach relatively large system sizes.

### III. NUMERICAL RESULTS

#### A. Self-correction transition

Starting from the toric code ground state and with all the CA field initialized to zero, we simulate the dynamics from Eq. (6). The most interesting regime is character-

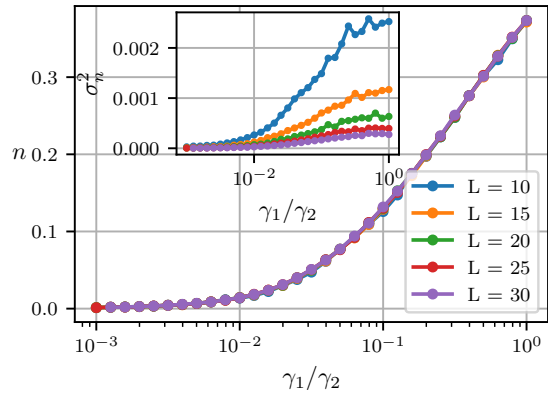


FIG. 3. Mean anyon density  $n$  for various system sizes  $L \times L$  as a function of the error rate  $\gamma_1$ . The inset depicts the variance of the anyon density  $\sigma_n^2$ . The variance decreases with increasing system size.

ized by the inequalities  $\gamma_1 \ll \gamma_2 \ll \gamma_3$ , which leaves the possibility for successful suppression of errors in the long-time limit.

A central challenge in the simulation of such open systems is that we are interested both in the long-time limit and the thermodynamic limit at the same time, which generically do not commute with each other [66]. To address this, we identify the timescale on which logical errors start to appear. Under diffusive dynamics of the anyons, this will happen on a timescale of  $t \sim L^4/\gamma_1$ , which indicates how the simulation time has to be adapted if the system size is changed to ensure that the system has converged to its steady state. We have numerically checked the validity of this scaling. The results are then obtained from averaging over  $10^3$  trajectories.

In Fig. 2, we show the logical error probability obtained for various anyon-pair creation rates. We fix  $\gamma_3 = 10\gamma_2$ . We notice that for  $\gamma_1 < 10^{-2}\gamma_2$ , the probability of a logical error falls rapidly, and this suppression persists for longer times as the system size increases. For  $\gamma_1 > 10^{-2}\gamma_2$ , the logical errors occur with certainty in the long-time limit. As the system size scales up, we clearly observe the critical error rate converging to approximately  $\gamma_1 = 10^{-2}\gamma_2$ . This establishes the existence of a phase transition between a phase where self-correction of errors is possible and a second trivial phase where logical errors prevent self-correction. Strikingly, we observe this feature even though our CA field is only two-dimensional, which is not sufficient to obtain a finite threshold in the conventional error correction setting [52]. From this we conclude that the time-continuous nature of the Lindblad dynamics further stabilizes the error correction properties of the toric code [62].

Below the critical rate, the anyons are still sparse and the CA generates a field that pairs them correctly without having to cross the boundary. Interestingly, we find that the density of anyons is a smooth function across the

critical point, see Fig. 3, which does not show significant finite-size corrections. However, as shown in the inset, this is not true for the variance, which strongly decreases under finite-size scaling, although it appears to reach a finite value in the trivial phase.

### B. Relationship to topological order

Let us now turn to the question how the self-correction transition is related to the topological order of the system. For this, we turn to an operational definition of topological order [58], which can also be readily applied for open quantum systems. Specifically, we compute the depth of a classical error correction circuit to correct the system back into one of the ground states of the toric code. The concrete implementation associates with each measured error a walker that explores its surroundings to fuse with other errors [67]. Then, if the depth is sufficiently short, we conclude that the system is in its topologically ordered phase.

In Fig. 4a, we show the mean circuit depth as a function of  $\gamma_1$ , normalized to the system size  $L^2$ . As expected, we observe a qualitative change in the finite-size scaling behavior when crossing the self-correction transition. At small  $\gamma_1$  before the transition, there is a data collapse of all system sizes onto a single line. After the transition, there is a region of superlinear growth of the circuit depth. Remarkably, the normalized circuit depth being constant in the self-correcting phase implies that the unnormalized circuit depth increases with the system size. This is a different situation compared to many other examples, where the circuit depth in the topological phase does not scale with the system size [58, 68–70]. Nevertheless, the growth with system size is not sufficient to cause logical errors, as the mean circuit depth only reaches a few percent of the total system size. This suggests that fluctuations of the circuit depth have to be sufficiently small, so they cannot induce logical errors in a significant fraction of the observed realizations. Indeed, as shown in Fig. 4b, the variance of the normalized circuit depth vanishes in the self-correcting phase, while it reaches a finite value following the phase transition. From this we conclude that the variance of the circuit depth is a better measure to determine the phase transition.

Turning to the operational definition also has a practical advantage. In the previous section, we have computed the logical error probability for the initial state being one of the toric code ground states. However, it is not possible to use a trivial initial state in this approach, as the value of the logical bit is not defined in this case. In contrast to this, the operational definition can be applied for arbitrary initial states. We have computed the circuit depth using the topologically trivial maximally mixed state as the initial state and obtain results that are indistinguishable from those presented in Fig. 4.

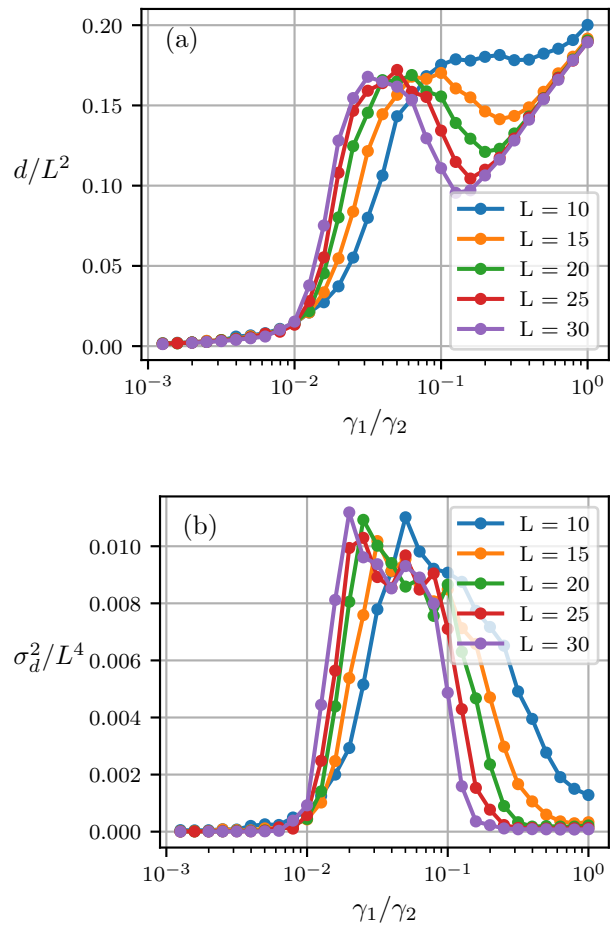


FIG. 4. (a) Mean circuit depth  $d$  normalized to the system size  $L \times L$  as a function of the error rate  $\gamma_1$  with fixed  $\gamma_3 = 10\gamma_2$ . Above the self-correction transition, the normalized circuit depth shows a modified scaling with system size. (b) Variance of the circuit depth  $\sigma_d^2$  normalized to the system size. Below the transition, the normalized variance vanishes in the thermodynamic limit, while it reaches a finite value after the transition.

### C. Steady-state phase diagram

We now obtain the entire phase diagram for different rates of the processes in the master equation using the operational definition. Using the error correction rate  $\gamma_2$  as a fixed reference, we compute the critical rate  $\gamma_1$  for the self-correction transition for different choices of the field-update rate  $\gamma_3$ . The shaded region in Fig. 5 corresponds to the self-correcting phase. Remarkably, we do not observe a monotonous behavior of the phase transition line, but rather a pronounced peak around an optimal field-update rate. While it can be readily understood that a slow field-update rate can be insufficient to provide the information for the anyons to move in the correct direction, the behavior for large  $\gamma_3$  deserves further explanation. We attribute the decrease in the critical  $\gamma_1$

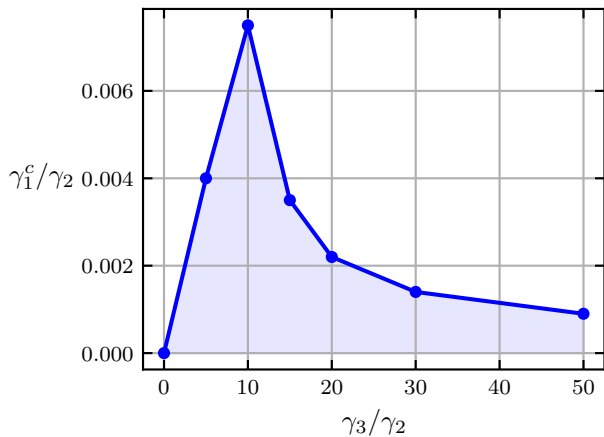


FIG. 5. Phase diagram depicting the critical error rate  $\gamma_1^c$  depending on the CA field-update rate  $\gamma_3$ . The shaded region indicates the self-correcting phase in which errors can successfully be corrected. This suggests an optimal rate of CA field-update beyond which the critical error rate starts declining.

to the fact that for large  $\gamma_3$ , the local field will also contain information from more distant anyons. However, the key notion behind error correction in the toric code is to

fuse all emerging anyon pairs in the same way they were originally created. Generically, anyons that are further apart are more likely to stem from a different anyon pair, making it unfavorable to move towards them and thus reducing the critical  $\gamma_1$ .

#### IV. CONCLUSION

In this work, we have analyzed a quantum master equation derived from a CA decoder for topological quantum error correction. Despite the update rules being strictly local, we find the existence of a self-correcting phase in the steady state of the dynamics. The decoding emerges from local, non-equilibrium dynamics of both the quantum system under consideration and the classical CA field. Our numerical simulations establish a self-correction threshold when the ratio between error generation and error correction rates is about 0.008.

From a practical implementation standpoint, our approach offers significant advantages for scalable quantum computing architectures. Unlike matching-based decoders, which often face a latency bottleneck as system sizes grow, the CA approach allows for  $\mathcal{O}(1)$  complexity per field-update. This locality permits the integration of decoding logic directly into the qubit control lines [71], significantly reducing the bandwidth requirements between the quantum plane and the classical control stack.

- 
- [1] M. A. Nielsen and I. L. Chuang, *Quantum computation and quantum information* (Cambridge University Press, 2010).
- [2] D. P. DiVincenzo, *Fortschr. Phys.* **48**, 771 (2000).
- [3] J. Preskill, *Proceedings of the Royal Society of London. Series A* **454**, 385 (1998).
- [4] J. Bausch, A. W. Senior, F. J. Heras, T. Edlich, A. Davies, M. Newman, C. Jones, K. Satzinger, M. Y. Niu, S. Blackwell, *et al.*, *Nature* **635**, 834 (2024).
- [5] N. Delfosse and N. H. Nickerson, *Quantum* **5**, 595 (2021).
- [6] P. Baireuther, T. E. O'Brien, B. Tarasinski, and C. W. J. Beenakker, *Quantum* **2**, 48 (2018).
- [7] B. M. Terhal, *Reviews of Modern Physics* **87**, 307 (2015).
- [8] S. Bravyi, M. Suchara, and A. Vargo, *Phys. Rev. A* **90**, 032326 (2014).
- [9] M. B. Hastings, [arXiv:1312.2546](https://arxiv.org/abs/1312.2546) (2013).
- [10] A. G. Fowler, M. Mariantoni, J. M. Martinis, and A. N. Cleland, *Phys. Rev. A* **86**, 032324 (2012).
- [11] G. Duclos-Cianci and D. Poulin, *Phys. Rev. Lett.* **104**, 050504 (2010).
- [12] D. Gottesman, *Stabilizer codes and quantum error correction* (California Institute of Technology, 1997).
- [13] S. Diehl, A. Micheli, A. Kantian, B. Kraus, H. P. Büchler, and P. Zoller, *Nature Physics* **4**, 878 (2008).
- [14] F. Verstraete, M. M. Wolf, and J. Ignacio Cirac, *Nature Phys.* **5**, 633 (2009).
- [15] H. Weimer, M. Müller, I. Lesanovsky, P. Zoller, and H. P. Büchler, *Nature Phys.* **6**, 382 (2010).
- [16] M. J. Hartmann, *Phys. Rev. Lett.* **104**, 113601 (2010).
- [17] S. Diehl, A. Tomadin, A. Micheli, R. Fazio, and P. Zoller, *Phys. Rev. Lett.* **105**, 015702 (2010).
- [18] D. Nagy, G. Kónya, G. Szirmai, and P. Domokos, *Phys. Rev. Lett.* **104**, 130401 (2010).
- [19] A. Tomadin, S. Diehl, and P. Zoller, *Phys. Rev. A* **83**, 013611 (2011).
- [20] T. E. Lee, H. Häffner, and M. C. Cross, *Phys. Rev. A* **84**, 031402(R) (2011).
- [21] E. M. Kessler, G. Giedke, A. Imamoglu, S. F. Yelin, M. D. Lukin, and J. I. Cirac, *Physical Review A* **86**, 012116 (2012).
- [22] M. Hönig, M. Moos, and M. Fleischhauer, *Phys. Rev. A* **86**, 013606 (2012).
- [23] L. M. Sieberer, S. D. Huber, E. Altman, and S. Diehl, *Phys. Rev. Lett.* **110**, 195301 (2013).
- [24] E. G. D. Torre, S. Diehl, M. D. Lukin, S. Sachdev, and P. Strack, *Phys. Rev. A* **87**, 023831 (2013).
- [25] T. E. Lee, S. Gopalakrishnan, and M. D. Lukin, *Phys. Rev. Lett.* **110**, 257204 (2013).
- [26] Z. Cai and T. Barthel, *Phys. Rev. Lett.* **111**, 150403 (2013).
- [27] H. Weimer, *Phys. Rev. Lett.* **114**, 040402 (2015).
- [28] M. Marcuzzi, M. Buchhold, S. Diehl, and I. Lesanovsky, *Phys. Rev. Lett.* **116**, 245701 (2016).
- [29] M. F. Maghrebi and A. V. Gorshkov, *Phys. Rev. B* **93**, 014307 (2016).
- [30] J. Jin, A. Biella, O. Viyuela, L. Mazza, J. Keeling, R. Fazio, and D. Rossini, *Phys. Rev. X* **6**, 031011 (2016).
- [31] J. Marino and S. Diehl, *Phys. Rev. Lett.* **116**, 070407 (2016).

- (2016).
- [32] A. Kshetrimayum, H. Weimer, and R. Orús, *Nature Commun.* **8**, 1291 (2017).
- [33] R. Rota, F. Storme, N. Bartolo, R. Fazio, and C. Ciuti, *Phys. Rev. B* **95**, 134431 (2017).
- [34] M. Buchhold, B. Everest, M. Marcuzzi, I. Lesanovsky, and S. Diehl, *Phys. Rev. B* **95**, 014308 (2017).
- [35] A. Nagy and V. Savona, *Phys. Rev. A* **97**, 052129 (2018).
- [36] F. Carollo, E. Gillman, H. Weimer, and I. Lesanovsky, *Phys. Rev. Lett.* **123**, 100604 (2019).
- [37] J. Panas, M. Pasek, A. Dhar, T. Qin, A. Geißler, M. Hafez-Torbati, M. E. Sorantin, I. Titvinidze, and W. Hofstetter, *Phys. Rev. B* **99**, 115125 (2019).
- [38] M. Raghunandan, F. Wolf, C. Ospelkaus, P. O. Schmidt, and H. Weimer, *Science Advances* **6**, eaaw9268 (2020).
- [39] F. Carollo and I. Lesanovsky, *Phys. Rev. Lett.* **128**, 040603 (2022).
- [40] V. P. Singh and H. Weimer, *Phys. Rev. Lett.* **128**, 200602 (2022).
- [41] C. D. Mink and M. Fleischhauer, *SciPost Phys.* **15**, 233 (2023).
- [42] L. M. Sieberer, M. Buchhold, J. Marino, and S. Diehl, *Rev. Mod. Phys.* **97**, 025004 (2025).
- [43] C. Wang, J. Harrington, and J. Preskill, *Annals of Physics* **303**, 31 (2003).
- [44] M. Sarovar, T. Proctor, K. Rudinger, K. Young, E. Nielsen, and R. Blume-Kohout, *Quantum* **4**, 321 (2020).
- [45] D. Aharonov, A. Kitaev, and J. Preskill, *Phys. Rev. Lett.* **96**, 050504 (2006).
- [46] C. D. Wilen, S. Abdullah, N. Kurinsky, C. Stanford, L. Cardani, G. d’Imperio, C. Tomei, L. Faoro, L. Ioffe, C. Liu, *et al.*, *Nature* **594**, 369 (2021).
- [47] S. Kumar and V. Tripathi, *Phys. Rev. B* **110**, L161111 (2024).
- [48] D. Vodola, M. Rispler, S. Kim, and M. Müller, *Quantum* **6**, 618 (2022).
- [49] F. Minganti, A. Biella, N. Bartolo, and C. Ciuti, *Physical Review A* **98**, 042118 (2018).
- [50] D. Roberts and A. A. Clerk, *Physical Review X* **10**, 021022 (2020).
- [51] C.-E. Bardyn, M. A. Baranov, C. V. Kraus, E. Rico, A. İmamoğlu, P. Zoller, and S. Diehl, *New Journal of Physics* **15**, 085001 (2013).
- [52] M. Herold, E. T. Campbell, J. Eisert, and M. J. Kastoryano, *npj Quantum Inf.* **1**, 15010 (2015).
- [53] M. Herold, M. J. Kastoryano, E. T. Campbell, and J. Eisert, *New Journal of Physics* **19**, 063012 (2017).
- [54] A. Kubica and J. Preskill, *Phys. Rev. Lett.* **123**, 020501 (2019).
- [55] M. Vasmer, D. E. Browne, and A. Kubica, *Scientific reports* **11**, 2027 (2021).
- [56] J. W. Harrington, *Analysis of quantum error-correcting codes: symplectic lattice codes and toric codes* (California Institute of Technology, 2004).
- [57] E. Dennis, A. Kitaev, A. Landahl, and J. Preskill, *Journal of Mathematical Physics* **43**, 4452 (2002).
- [58] A. Jamadagni and H. Weimer, *Phys. Rev. B* **106**, 085143 (2022).
- [59] Y.-J. Liu and S. Lieu, *Phys. Rev. A* **109**, 022422 (2024).
- [60] E. Kapit, J. T. Chalker, and S. H. Simon, *Phys. Rev. A* **91**, 062324 (2015).
- [61] S. Balasubramanian, M. Davydova, and E. Lake, *arXiv:2412.19803* (2025).
- [62] G. Dünneweber, G. Styliaris, and R. Trivedi, *arXiv:2601.20818* (2026).
- [63] A. Kitaev, *Annals of Physics* **303**, 2 (2003).
- [64] A. Kitaev, *Annals of Physics* **321**, 2 (2006).
- [65] A. Jamadagni, H. Weimer, and A. Bhattacharyya, *Phys. Rev. B* **98**, 235147 (2018).
- [66] H. Weimer, A. Kshetrimayum, and R. Orús, *Rev. Mod. Phys.* **93**, 015008 (2021).
- [67] J. Wootton, *Entropy* **17**, 1946 (2015).
- [68] A. Jamadagni and H. Weimer, *Phys. Rev. B* **106**, 115133 (2022).
- [69] A. Jamadagni, J. Kazemi, and H. Weimer, *Phys. Rev. B* **107**, 075146 (2023).
- [70] L. Fraatz, A. Jamadagni, and H. Weimer, *New Journal of Physics* **28**, 014512 (2026).
- [71] L. Caune, L. Skoric, N. S. Blunt, A. Ruban, J. McDaniel, J. A. Valery, A. D. Patterson, A. V. Gramolin, J. Majaniemi, K. M. Barnes, *et al.*, *arXiv:2410.05202* (2024).